E-type noncollinear magnetic ordering in multiferroic *o*-$LuMnO_3$

Saumya Mukherjee,[1,*] Andreas Dönni,[2] Taro Nakajima,[3,†] Setsuo Mitsuda,[3] Makoto Tachibana,[4] Hideaki Kitazawa,[2] Vladimir Pomjakushin,[1] Lukas Keller,[1] Christof Niedermayer,[1] Andrea Scaramucci,[5] and Michel Kenzelmann[5,‡]

[1]*Laboratory for Neutron Scattering and Imaging, Paul Scherrer Institut, 5232 Villigen PSI, Switzerland*

[2]*National Institute for Materials Science (NIMS), 1-2-1 Sengen, Tsukuba, Ibaraki 305-0047, Japan*

[3]*Department of Physics, Faculty of Science, Tokyo University of Science, Kagurazaka 1-3, Shinjuku-ku, Tokyo, Japan*

[4]*National Institute for Materials Science (NIMS), 1-1 Namiki, Tsukuba, Ibaraki 305-0044, Japan*

[5]*Laboratory for Scientific Developments and Novel Materials, Paul Scherrer Institut, CH 5232 Villigen-PSI, Switzerland*

(Received 20 September 2016; published 13 March 2017)

Multiferroic orthorhombic *o*-$LuMnO_3$ exhibits large ferroelectric polarization induced by an *E*-type magnetic order. Recently, the *E*-type magnetic phase in $LuMnO_3$ was proposed to feature magnetic moments tilted away from the *collinear* ordering. We employed neutron diffraction to determine the symmetry of the magnetic order in *o*-$LuMnO_3$. We observed that below $T_N = 39$ K, the Mn^{3+} spins order into an incommensurate amplitude-modulated phase that obeys the *Pbnm* crystal symmetry and is paraelectric. The incommensurate phase locks into a commensurate phase at $T_C = 35.5$ K described by a fully antiferromagnetic and *noncollinear* *E*-type order. This *noncollinear* *E*-type ordering breaks the spatial inversion symmetry and induces a spontaneous polarization at T_C. At $T = 2$ K, an appreciably large electric polarization was observed similar to that of other orthorhombic manganites featuring *E*-type magnetic order. We also present a *Pbnm* symmetry-allowed Dzyaloshinskii-Moriya interaction that explains the *noncollinear* *E*-type order in the commensurate phase. These results are in qualitative agreement with the type of distortions from *collinear* *E*-type antiferromagnetic order found using Monte Carlo simulation for rare-earth manganites [M. Mochizuki *et al.*, Phys. Rev. B **84**, 144409 (2011)].

DOI: 10.1103/PhysRevB.95.104412

I. INTRODUCTION

Magnetoelectric (ME) multiferroics are a unique class of materials that can simultaneously host both magnetic and ferroelectric orders [1]. The coupling of such switchable order parameters generated enormous interest due to the possibility of developing new types of materials for spintronics and memory devices [2,3]. A direct magnetoelectric coupling was observed in rare-earth (*R*) manganites with magnetic order inducing spontaneous ferroelectricity [4]. This is different from other multiferroic materials such as $BiFeO_3$ [2], in which independent mechanisms stabilize the magnetic and electric orders. Orthorhombic $TbMnO_3$ is a prominent example of a multiferroic where ferroelectricity is driven by the antisymmetric exchange interactions of Mn spins [5,6], leading to a cross-coupling of magnetic and ferroelectric properties [7,8]. The limitation of the spin-spiral driven ferroelectricity is the relatively small polarization ($\leqslant 1000\ \mu C/m^2$) [6], which is due to the weak spin-orbit interaction.

Alternatively, larger ferroelectric polarizations ($\approx$1500–2400 $\mu C/m^2$) were observed in the commensurate phase of *o*-$RMnO_3$ (R = Tm,Ho) with modulation wave vector $q_b = 0.5$ and in the incommensurate phase of *o*-$YMnO_3$ with $q_b = 0.435$, where the Mn^{3+} spins ordered *collinearly* [9–13]. The observed enhancement of polarization (P) was attributed to symmetric exchange interactions [14]. Interestingly, recent multiferroic studies on $TbMnO_3$ under hydrostatic pressure showed enormously large polarization $P \approx 10\,000\ \mu C/m^2$ at 5.2 GPa in the commensurate magnetic phase [15]. The commensurate phase under high pressure of 5 GPa demonstrated a *collinear* *E*-type ordering, which confirmed the proposed *E*-type spin-driven ferroelectricity in $TbMnO_3$ [16].

Recent Monte Carlo investigations of a realistic spin model of $RMnO_3$ [14] show that the *collinear* *E*-type magnetic order might be strongly distorted due to interactions with spin-orbit origin. In this model, two possible interactions were considered to be responsible for the *noncollinear* deformation of the *E*-type spin structure.

One is the single-ion anisotropy $\mathcal{H}^E_{\rm sia}$ in the *ab* plane, and the other is the Dzyaloshinskii-Moriya interaction $\mathcal{H}_{\rm DM}$. For exchange couplings giving rise to a spiral state, $\mathcal{H}^E_{\rm sia}$ was shown to be responsible for an elliptically deformed *ab*-plane cycloid, while a similar deformation was also caused by the $\mathcal{H}_{\rm DM}$ interactions. For exchange couplings giving rise to *E*-type commensurate order, the temperature dependence of the average value of the two terms $\mathcal{H}^E_{\rm sia}$ and $\mathcal{H}_{\rm DM}$ indicates that single-ion anisotropy plays a major role in inducing the *noncollinearity* of the *E*-type phase. Indeed, below the transition from the spin density wave state to the *E*-type state, $\langle\mathcal{H}^E_{\rm sia}\rangle$ decreases with decreasing temperature while $\langle\mathcal{H}_{\rm DM}\rangle$ stays constant. Therefore, the single-ion anisotropy $\mathcal{H}^E_{\rm sia}$ was presented to be responsible for the deformation of *E*-type order, which, in the results presented in Ref. [14], mainly occur in the *ab* plane of the magnetic *R* ion. Nonetheless, the values of Dzyaloshinskii-Moriya couplings and single-ion anisotropy used in the study were based on estimations for $LaMnO_3$. The difficulty in obtaining accurate values for such small couplings and their possible dependence on the rare-earth ion leaves room for a different scenario in which the Dzyaloshinskii-Moriya interactions might have a prominent role with respect to the single-ion anisotropy. Therefore, it is desirable to identify experimental features that indicate whether $\mathcal{H}^E_{\rm sia}$ or $\mathcal{H}_{\rm DM}$ might have a dominant role.

*saumya.mukherjee@psi.ch

†Present address: RIKEN Center for Emergent Matter Science (CEMS), Wako 351-0198, Japan.

‡michel.kenzelmann@psi.ch

In this work, we use neutron scattering to investigate the magnetic order of $LuMnO_3$. In contrast to some of the other E-type multiferroics [9,13,17], we find a small canting of the moments. In this *noncollinear* E-type antiferromagnetic order, the main components of the magnetic moments are in the bc plane. We analyze the symmetry of the magnetic order and verify the *noncollinear* E-type model proposed for $RMnO_3$. We discuss our results in view of the model presented in Ref. [14]. We find that the discrepancy between the proposed model and the experimentally observed magnetic moments can be explained with a dominant role of $\mathcal{H}_{\rm DM}$ with respect to a smaller contribution of $\mathcal{H}^E_{\rm sia}$. Moreover, we present the ferroelectric properties of $LuMnO_3$ and compare them with previous reports of a large ferroelectric polarization $P_o \approx 4600\ \mu C/m^2$ and theoretical predictions (up to 6000 $\mu C/m^2$ at 0 K) [18,19]. We discuss o-$LuMnO_3$ as a multiferroic oxide with large ferroelectric polarization induced by a commensurate *noncollinear* E-type Mn^{3+} spin ordering. We note that, among o-$RMnO_3$ exhibiting ferroelectricity from E-type magnetic order, o-$LuMnO_3$ is an ideal model system to study the ordering of Mn^{3+} spins due to the absence of the magnetic R ion.

II. SAMPLES AND CHARACTERIZATIONS

Polycrystalline samples of orthorhombic $LuMnO_3$ were prepared under high pressure as described in Ref. [20]. Neutron powder diffraction measurements were performed using ≈5 g of the $LuMnO_3$ sample using the HRPT [21] and DMC diffractometers at the Paul Scherrer Institut, SINQ (Switzerland) with incident neutrons of wavelength 1.89 and 4.5 Å, respectively. Magnetic structure refinements were performed using the FULLPROF suite [22]. The symmetry analysis was performed using the ISODISTORT tool based on the ISOTROPY software [23,24] and the `BasiRep` program [22]. The ferroelectric polarization was determined using a 0.43 mm thin hardened pellet of polycrystalline $LuMnO_3$ covered with a 6.03×10^{-6} m^2 area of silver epoxy. The sample was cooled from $T = 50$ to 2 K in poling electric fields of up to $E_p = 3000\ kV/m$, after which the electric field was reduced to zero and the sample was allowed to discharge for 1000 s. After the discharge at $T = 2$ K, the residual current was reduced to 10^{-14} A, suggesting that the pyroelectric measurements were not affected by trapped charges. The pyroelectric current was measured using a Keithley 6517 A electrometer with increasing temperature and at different ramping speeds. To verify the absence of contributions of trapped charges to the pyrocurrent, stop and go ramped pyroelectric measurements were performed [9]. The temperature dependence of polarization is identical for different ramping sequences. This confirms that trapped charges do not affect the pyroelectric current measurements. The real and imaginary coefficients of the dielectric constant were measured using an Agilent E4980A LCR meter. Frequency-dependent measurements confirm that the Maxwell-Wagner effect does not affect the measurements.

III. RESULTS AND DISCUSSION

A. Structural properties

$LuMnO_3$ crystallizes in the orthorhombic $Pbnm$ space group and has the following lattice parameters: $a = 5.2023$ Å, $b = 5.7839$ Å, and $c = 7.3137$ Å, obtained from refinement of the nuclear reflections at room temperature $T = 300$ K. The chemical unit cell contains four magnetic Mn^{3+} ions, located at $\mathbf{r}_1 = (0.5,0,0)$, $\mathbf{r}_2 = (0,0.5,0)$, $\mathbf{r}_3 = (0.5,0,0.5)$, and $\mathbf{r}_4 = (0,0.5,0.5)$. The refined crystal structure is in good agreement with the earlier studies [17]. Inherent to the $RMnO_3$ perovskite crystal structure, $LuMnO_3$ experiences a large $GdFeO_3$-type distortion due to the smaller radii of the Lu ion [25,26]. This induces a large deviation of the Mn-O-Mn bond angle away from 180° as observed in the series of $RMnO_3$ with small R ion sizes [27]. This reduces the frustration among the competing spin states and stabilizes a commensurate magnetic structure in o-$LuMnO_3$.

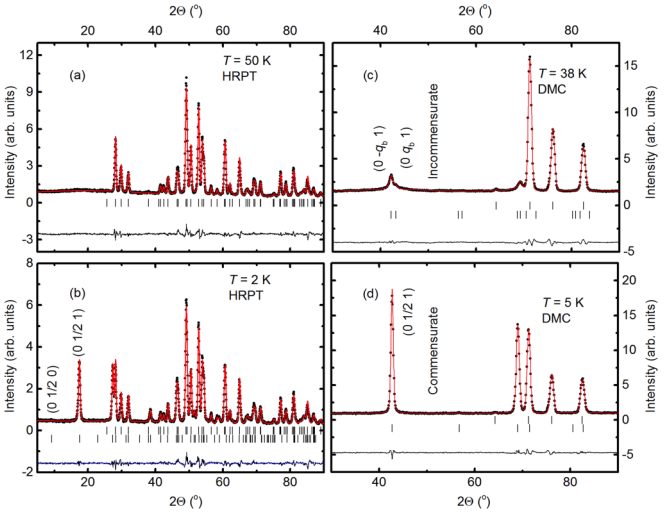

FIG. 1. Powder neutron scattering patterns from $LuMnO_3$ measured using HRPT as a function of scattering angle 2Θ at (a) $T = 50$ K showing only nuclear scattering, and (b) $T = 2$ K showing additional magnetic peaks such as (0, 1/2, 0) and (0, 1/2, 1). (c,d) Bragg peak powder patterns measured using DMC at $T = 38$ and 5 K. (a)–(d) The vertical bars indicate magnetic and nuclear (upper row) Bragg peaks. The bottom solid line indicates the difference between the experiment and the model.

B. Magnetic properties

Neutron diffraction studies on the o-$LuMnO_3$ powder sample are presented in Fig. 1. At $T = 50$ K, a nonmagnetic phase was observed with nuclear reflections originating from the chemical lattice [Fig. 1(a)]. On cooling to $T = 38$ K, we observed additional magnetic reflections, for example at the $(0,\pm q_b,1)$ wave vectors [Fig. 1(c)]. The magnetic reflections showed an incommensurate magnetic ordering with wave vector $\mathbf{Q} = (0,q_b,0)$, where q_b is the magnetic modulation wave number along the **b** axis. In the incommensurate phase, we observed that $q_b \neq 0.5$. At $T = 5$ and 2 K, the incommensurate reflections were absent. In fact, the magnetic reflections such as $(0,1/2,0)$ and $(0,1/2,1)$ with commensurate ordering were observed [Figs. 1(b) and 1(d)].

The powder diffraction patterns with magnetic Bragg peaks $(h,k \pm q,l)$ were fitted to scattering patterns expected for various magnetic structures. Representation analysis was used to restrict the number of free parameters and to find

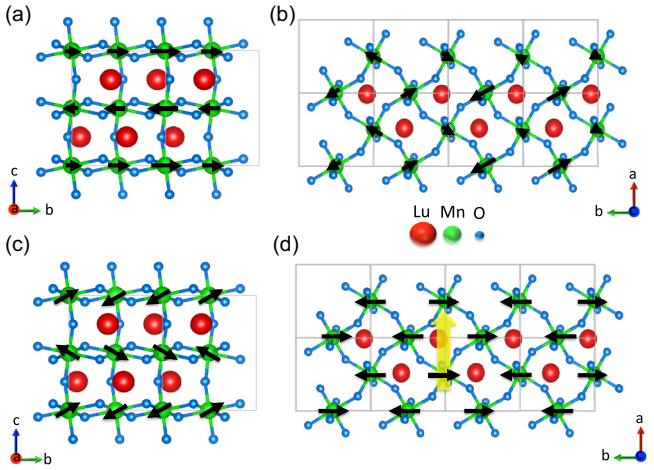

FIG. 2. Schematic illustrations of the magnetic structure (a), (b) at $T_C = 35.5 < T < T_N = 39$ K and (c),(d) at $T < T_C$ projected onto the *bc* plane and the *ab* plane, respectively. In the amplitude-modulated incommensurate phase (a),(b) the Mn^{3+} spins are oriented along the **b** axis and tilted toward the **a** axis. In the commensurate phase (c),(d) the spins ordering with the *noncollinear* E_1 type are shown. The spins in the *noncollinear* E_1 type are shown tilting away from the **b** axis toward the **c** axis ($\theta \sim \pm 3.9^\circ$). It violates the inversion symmetry along the **a** axis inducing a ferroelectric polarization below T_C along the **a** axis, (d) $+P_a(E_1)$ (yellow arrows). Here, the tilting and magnitude of moments are exaggerated as a guide to eye.

the irreducible representations that describe the magnetic structures. It was found that the magnetic structure in the high-temperature incommensurate (HTI) phase is described by a single irreducible representation (irrep). The best fit was obtained with $\chi^2 = 5.21$ for a structure described by the representation $\Gamma^3_{\rm IC}$ according to Kovalev's notation [28], and it is defined by the following characters: $\chi(I) = 1$, $\chi(2_b) = -\alpha$, $\chi(m_{bc}) = -\alpha$, and $\chi(m_{ab}) = 1$ with $\alpha = \exp(i\pi q)$. The magnetic structure is described by one single-order parameter with an amplitude given by $m^3_{\rm IC} = \sqrt{2}\,[0.54(4),1.28(2),0.00(3)]\mu_B$ of the Mn^{3+} ions at $T = 38$ K with basis vectors identical to the incommensurate order in $TmMnO_3$ [9]. Here the superscript 3 denotes the irrep and subscript IC signifies the incommensurate phase. The magnetic structure in the HTI phase is amplitude-modulated with moments *collinear* in the *bc* plane [Fig. 2(a)], forming an angle ($\approx \pm 23^\circ$ at $T = 38$ K) with the **b** axis in the *ab* plane [Fig. 2(d)].

The magnetic structure in the low-temperature commensurate (LTC) phase is described by a two-dimensional irrep. At $T = 2$ K, the best agreement was achieved with $\chi^2 = 2.94$ for the magnetic ordering involving Γ^1_C [28] defined by the nonzero characters: $\chi(I) = 2$ and $\chi(m_{ab}) = 2$. The magnetic moments of the Mn^{3+} ions were found to be *noncollinear* and lying in the *bc* plane, with $m^1_C = [0.00(2),3.67(1),0.25(2)]\mu_B$ at $T = 5$ K, where the subscript *C* signifies the commensurate phase [Figs. 2(c) and 2(d)]. Importantly, the magnetic structure differs from the magnetic structure in the commensurate phase of $TmMnO_3$ [9], and from a previously reported magnetic structure of $LuMnO_3$ [17], where the moments of the Mn^{3+} ions are completely collinear along the **b** axis. The moments were observed to be tilted in the *bc* plane forming an angle $\theta = \pm 3.9^\circ$ with the **b** axis at $T = 5$ K [Fig. 2(c)]. In the *ab* plane, the moments are aligned along the **b** axis [Fig. 2(d)].

The magnetic order in the LTC phase can be described by *noncollinear* *E*-type antiferromagnetic ordering with *noncentrosymmetric* orthorhombic magnetic space group P_bmn2_1 (no. 31.129 in BNS settings). For these settings, the Mn^{3+} positions and magnetic moments are (3/4,5/8,1/2,0.25(2),3.67(1),0.00(2)). There are four antiferromagnetic domains with such *E*-type magnetic ordering. These can be grouped in two pairs of domains. Domains in the same pair transform one into the other by time reversal (e.g., reversing all the sublattice magnetizations). The first pair of domains have E^b_1-type staggered magnetization along **b** and O^c_1-type staggered magnetization along **c** (see Table I). These correspond to the bases choice $\mathbf{a}' = \mathbf{c}$, $\mathbf{b}' = 2\mathbf{b}$, and $\mathbf{c}' = -\mathbf{a}$ and, respectively, to the origin shift $\mathbf{p} = \frac{3}{4}\mathbf{b} + \frac{1}{4}\mathbf{c}$ and $\mathbf{p} = \frac{7}{4}\mathbf{b} + \frac{1}{4}\mathbf{c}$, where $\mathbf{a}'$, $\mathbf{b}'$, and $\mathbf{c}'$ are the lattice constants in the P_bmn2_1 settings. The second pair is composed by the domains with staggered magnetization along **b** of the E^b_2-type and O^c_2-type staggered magnetization along **c**. These correspond to the bases choice $\mathbf{a}' = -\mathbf{c}$, $\mathbf{b}' = 2\mathbf{b}$, and $\mathbf{c}' = \mathbf{a}$ and, respectively, to the origin shift $\mathbf{p} = \frac{1}{2}\mathbf{a} + \frac{5}{4}\mathbf{b} + \frac{1}{4}\mathbf{c}$ and $\mathbf{p} = \frac{1}{2}\mathbf{a} + \frac{9}{4}\mathbf{b} + \frac{1}{4}\mathbf{c}$. Elements of the first pair transform into elements of the second pair by the inversion symmetry of the paramagnetic space group $Pbnm$.

The magnetic spin structure in the LTC phase has no net magnetization, and the ordering of magnetic moments along **a**, **b**, and **c** is summarized in Table I. The absence of magnetic intensity on Bragg peaks that are sensitive to ferromagnetic canting of Mn^{3+} spins (Fig. 1) confirms that the LTC antiferromagnetic (AFM) phase has no ferromagnetic component. The canting of spins in the *bc* plane generates

TABLE I. Domains of the *E*-type order parameter (O.P.).

O.P.	Sublattice magnetization	Mn_1 (0.5 0 0)	Mn_2 (0 0.5 0)	Mn_3 (0.5 0 0.5)	Mn_4 (0 0.5 0.5)	Mn_5 (0.5 1 0)	Mn_6 (0 1.5 0)	Mn_7 (0.5 1 0.5)	Mn_8 (0 1.5 0.5)
	E^a_1	0	0	0	0	0	0	0	0
E_1	E^b_1	m^b	$-m^b$	$-m^b$	m^b	$-m^b$	m^b	m^b	$-m^b$
	O^c_1	m^c	$-m^c$	m^c	$-m^c$	$-m^c$	m^c	$-m^c$	m^c
	E^a_2	0	0	0	0	0	0	0	0
E_2	E^b_2	m^b	m^b	$-m^b$	$-m^b$	$-m^b$	$-m^b$	m^b	m^b
	O^c_2	m^c	m^c	m^c	m^c	$-m^c$	$-m^c$	$-m^c$	$-m^c$

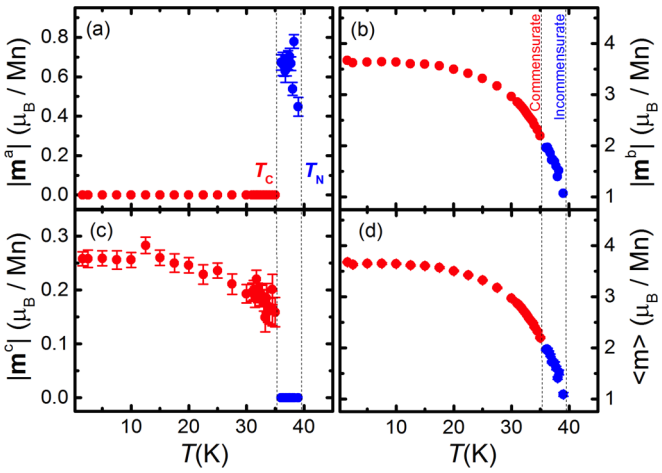

FIG. 3. Temperature dependence of the Mn^{3+} moment (a) $|m^a|$, (b) $|m^b|$, (c) $|m^c|$, and (d) the magnitude of the total moment with varying temperature. In the incommensurate phase, the magnitude is scaled by $\sqrt{2}$. The vertical dotted lines indicate the $T_C = 35.5$ K and $T_N = 39$ K.

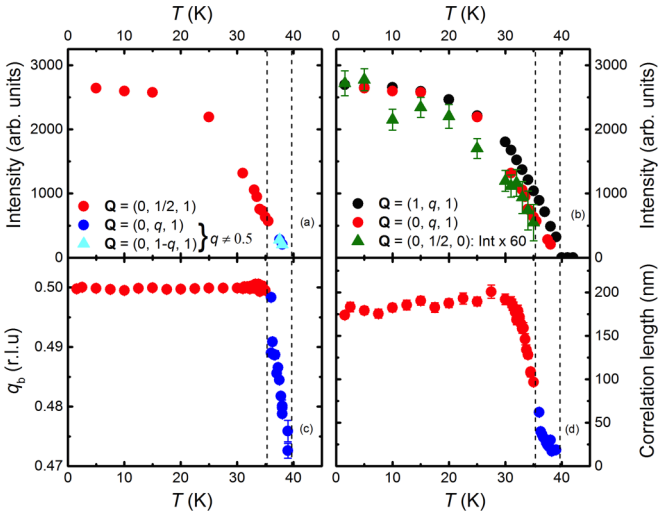

FIG. 4. (a) Temperature dependence of the magnetic Bragg peak intensity at $\mathbf{Q} = (0,1/2,1)$ in the commensurate phase and the intensities at the $\mathbf{Q} = (0,q,1)$ and $\mathbf{Q} = (0,1-q,1)$ Bragg peak positions for $0.47 < q \leqslant 0.5$. (b) Comparison of the temperature dependence of magnetic reflections $(0,q,1)$ and $(1,q,1)$. (c) Temperature dependence of the magnetic wave vector, q, along the **b** axis. (d) Temperature dependence of the magnetic correlation length. The vertical dotted lines indicate $T_C = 35.5$ K and $T_N = 39$ K.

a *noncollinear* ordering in contrast to multiferroics with a canted-AFM phase leading to weak ferromagnetism [29–31]. The observed *noncollinear* E-type ordering is in agreement with the *noncollinearity* of Mn^{3+} spins neighboring along the **c** direction, as discussed by Mochizuki *et al.* [14].

The temperature dependence of the components of moments along the **a**, **b**, and **c** crystallographic axes was obtained from the refinement of the powder diffraction data, and it is shown in Fig. 3. These data were measured while cooling the sample. The dominant magnetic component points along the **b** axis in both the HTI and LTC phases. In the HTI phase, there is an additional magnetic component along the **a** axis that at T_N is almost as large as the moment along the **b** axis. At T_C, the magnetic component along the **a** axis switches along the **c** axis. The variation of the magnitude of the Mn^{3+} spin moment $\langle m \rangle$ is shown in Fig. 3(d). It was observed to increase sharply in the incommensurate phase, but below T_C its increase slows down and around $T = 10$ K it saturates to $\approx 3.65 \mu_B$.

The satellite magnetic reflections $(0,q,1)$, $(0,1-q,1)$, and $(1,q,1)$ with $q \neq 0.5$ were observed to have identical behavior at $T_C = 35.5 < T < T_N = 39$ K, as shown in Figs. 4(a) and 4(b). Below T_C in the commensurate phase, the integrated intensities of the strongest magnetic reflections in the E-type phase $(0,1/2,1)$ and $(1,1/2,1)$ were observed to follow closely a similar temperature dependence [Figs. 4(a) and 4(b)]. In fact, the intensity of the weak $(0,1/2,0)$ reflection when scaled by a factor 60 also matches the temperature dependence of the $(0,1/2,1)$ and $(1,1/2,1)$ reflections. We also present the temperature dependence of the wave number q_b [Fig. 4(c)], and the magnetic correlation length in the incommensurate and commensurate phase [Fig. 4(d)]. The wave number q_b in the incommensurate phase changes rapidly as a function of temperature for $T > T_C = 35.5$ K, but in the commensurate phase it locks to $q_b = 0.5$ at T_C [Fig. 4(c)]. The observed transitions at T_N and T_C are in excellent agreement with the peaks observed in the temperature dependence of the specific heat [20]. The magnetic correlation length derived from the width of $(0,q,1)$ reflections never exceeds 200 nm even in the LTC phase [Fig. 4(d)]. This indicates a very small magnetic domain size and a very high density of domain walls.

We note that the emergence of the $(0,1/2,0)$ reflection in the commensurate phase of o-$LuMnO_3$ is purely due to the Mn^{3+} spin ordering, unlike in the commensurate phase of o-$TbMnO_3$ under high pressure [16,32], where the onset of the $(0,1/2,0)$ reflection was suggested to originate from the Tb^{3+} ordering. The $(0,1/2,0)$ reflection in $LuMnO_3$ emerges already at $T_C = 35.5$ K so that the commensurate phase of $LuMnO_3$ exhibits a *noncollinear* E-type ordering of Mn magnetic moments.

C. Electrical properties

Our measurements of the electric properties are summarized in Fig. 5. The temperature dependence of the real part of the dielectric susceptibility, ε_r' [Fig. 5(a)], indicates the onset of a polar ordering at $T = 35.5$ K, which coincides with the stabilization of the LTC *noncollinear* E-type state at T_C.

The first-order transition from the paraelectric to the ferroelectric phase at T_C results in the onset of spontaneous polarization [Figs. 5(a)–5(c)]. The spontaneous polarization was observed to increase monotonically in magnitude upon cooling below T_C. However, at $T < 6$ K a saturation in the polarization was reached [Fig. 5(c)]. This is coincident with the presence of the humplike feature in the temperature dependence of ε_r''. It is worth mentioning that the electric polarization (P) successfully demonstrated poling under an applied E field [Fig. 5(c), inset].

Next, we studied the effect on the polarization size when cooled under different electric (E) fields. The temperature dependence of the spontaneous polarization shows an increase with increasing E field [Fig. 5(d)]. $P(T)$ under different E fields was scaled by the polarization measured at 2 K [Fig. 5(e)]. The functional form of the $P(T)$ has a weak

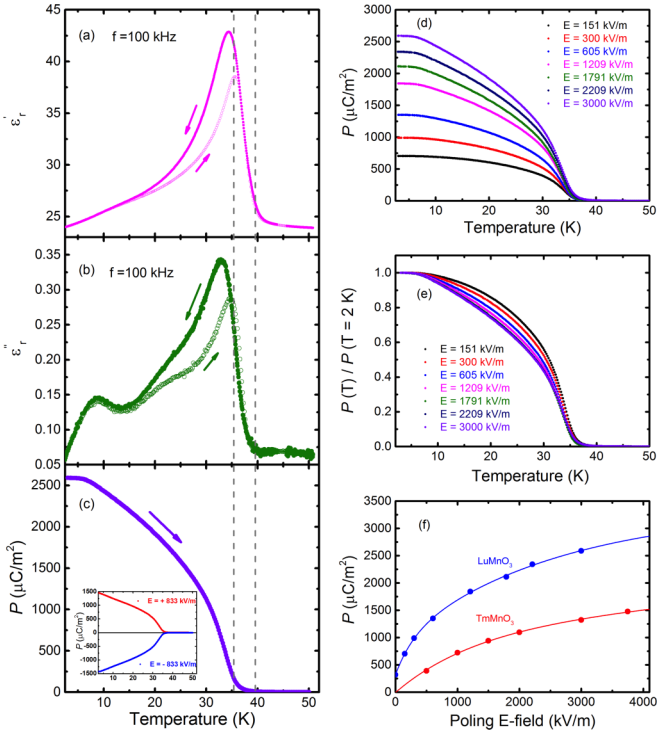

FIG. 5. (a), (b) Temperature variations of the real and imaginary parts of dielectric constants, ε_r' and ε_r'', respectively, measured at a frequency $f = 100$ kHz on cooling (solid circle) and warming (open circle). (c) T variation of the spontaneous electric polarization (P) measured after electric field cooling of $E_p = 3000$ kV/m. The dotted lines mark T_N and T_C. Inset: Switching of the ferroelectric polarization with a poling electric field of $|E| = 833$ kV/m is shown. (d) T variations of P after cooling under different applied E fields. (e) T variations of the P normalized to the value at $T = 2$ K. (f) Poling E-field dependence of the electric polarization magnitude at $T = 2$ K for $LuMnO_3$ and $TmMnO_3$ [9]. The lines are guides to the eye. The vertical dotted lines indicate T_C and T_N.

dependence on the applied E field. However, the temperature dependence of $P(T)/P(T = 2\ \text{K})$ clearly shows a slight increase within the temperature range of $10 < T < 30$ K with a decrease in the E field. A comparison of E-field dependent polarization $P(E)$ [Fig. 5(f)] at 2 K between o-$LuMnO_3$ and o-$TmMnO_3$ [9] shows that the electric polarization P in $LuMnO_3$ is found to be almost double that of $TmMnO_3$.

Large polarization, $P \approx 2600\ \mu\text{C/m}^2$, was observed for the polycrystalline $LuMnO_3$ with a poling electric field $E = 3000$ kV/m under ambient pressure at $T = 2$ K. An intrinsic value $P_o \approx 5200\ \mu\text{C/m}^2$ was estimated for the single crystalline phase considering it should be almost double the polarization in the polycrystalline phase. The achieved polarization $P(E)$ at $T = 2$ K was limited by the applied E field to our disposal.

The large polarization is also a good indication of the better sample quality essential for the polarization studies. The P_o obtained here is comparable to previous studies [12,19] and is in good agreement with the theoretically predicted $P_o \approx 4600\ \mu\text{C/m}^2$ for $R\text{MnO}_3$ with an E-type magnetic order originating from the symmetric exchange striction of the spin-lattice coupling [14].

In the imaginary part of the dielectric susceptibility ε_r'' [Fig. 5(b)] we observed a humplike feature at $T_A = 8$ K beside the peak at T_C. No anomaly has been observed in the specific heat [20], and the ε_r'' peak appears with a reduced maximum intensity (28%) compared to the ε_r'' peak at T_C. This broad peak cannot be caused by the R magnetism since Lu is nonmagnetic. In contrast, the magnetic Tm moments in $TmMnO_3$ lead to the release of additional magnetic entropy (small peak in the specific heat) [20], to an anomaly in the magnetic susceptibility (Ref. [9]) and an enhanced maximum intensity of the ε_r'' peak at T_A reaching 69% of the ε_r'' peak at T_C. We notice that at some lower temperature, there is an anomaly in the temperature dependence of the lattice parameters, suggesting an instability of the chemical lattice. Synchrotron radiation diffraction would be required to study the lattice changes in this low temperature in more detail.

We propose that the broad peak at T_A is related to the dynamics of domain walls. The movement of domain walls across the boundaries is facilitated by the absorption of energy, which in turn can induce a broad peak in the temperature dependence in the imaginary part of the dielectric susceptibility [33]. In fact, the dielectric constant shows a weak frequency dependence (not shown) that is qualitatively in agreement with the presence of domain walls. A relatively small correlation length suggests a smaller domain size and hence a higher density of domain walls. The domain walls are expected to have multiferroic character. Further studies, such as dielectric measurements under high magnetic fields, will be necessary to confirm the existence of the multiferroic domain walls.

To obtain independent evidence for spin-phonon coupling in o-$LuMnO_3$, we studied the temperature dependence of the lattice parameters (a,b,c) (Fig. 6). The lattice parameters a and c decrease, whereas the b-axis parameter increases slightly below T_C. The temperature dependence of the b lattice parameter is evidence that magnetic interactions along the b axis play a crucial role in the magnetic properties. A likely scenario is that magnetic frustration is relieved through a decrease of the a/b and c/b ratios in lattice parameters.

Unlike o-$TmMnO_3$ [9], the change in the lattice constants and the unit-cell volume (V) across the magnetic phase

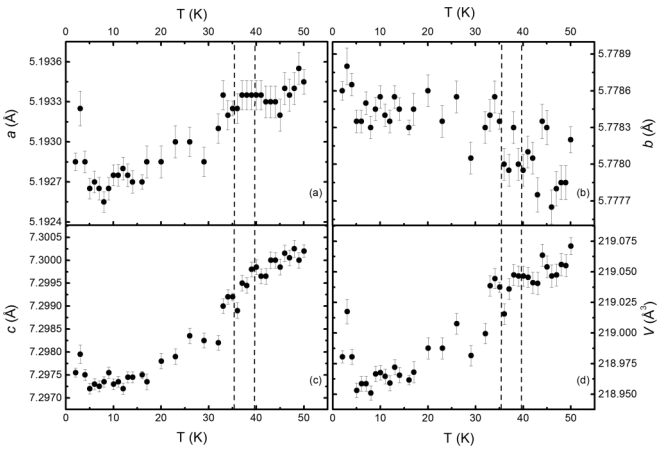

FIG. 6. Temperature dependence of the lattice constants for $T < 50$ K. The vertical dotted lines at $T_N = 39$ K and $T_C = 35.5$ K indicate the onset temperature for incommensurate and commensurate Mn spin ordering, respectively.

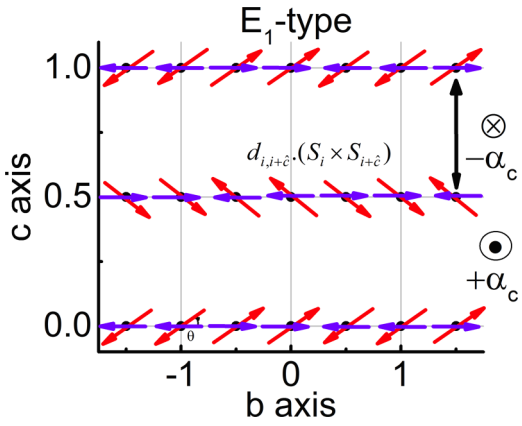

FIG. 7. Schematic of the spin structure in the E_1 domain projected on the *bc* plane. Blue arrows here resemble the collinear **c**-axis spin component. The DMI coupling parameter α_c switches sign along the **c** axis.

transitions at $T_C = 35.5$ K and $T_N = 39$ K lacks a clear anomaly. Below $T = 5$ K, a sharp jump in the lattice parameters falls in the region where a humplike feature was observed in the imaginary part of the electrical susceptibility.

D. Discussion

A Landau free-energy analysis was performed to explain the paraelectric HTI phase and the ferroelectric *noncollinear* LTC phase, in agreement with Picozzi *et al.* [34] for *collinear* *o*-$HoMnO_3$. The phenomenological explanation of the multiferroic behavior in *o*-$TbMnO_3$ was presented separately by Kenzelmann *et al.* [5] and by Mostovoy [35]. In the LTC phase, the transformations of the *Pbnm* space group leave the magnetoelectric coupling [34] between order parameter and electric polarization, $P^a(E_1^2 - E_2^2)$ (see the Appendix), invariant for polarization along the *a* axis. This is consistent with the generally accepted understanding of the allowed orientation of the polarization axis for the *collinear* *E*-type phase of *o*-$R MnO_3$ [36]. In summary, the *noncollinear* *E*-type phase follows the same symmetry transformations as that of the *collinear* *E*-type phase [34].

Here, we propose a scenario to explain the microscopic origin of the observed *noncollinear* magnetic ordering of the LTC phase based on the symmetry properties of a Dzyaloshinskii-Moriya (DM) interaction vector in the crystal structure of $RMnO_3$. This approach is supported by previous MC simulations performed by Mochizuki *et al.* in Refs. [14,37] on a spin model for $RMnO_3$. Within this model, we considered a DM vector that is allowed by the crystallographic symmetry [38] of $RMnO_3$. As in our measurements, we observed components of moments lying within the *bc* plane (Fig. 7), and we discuss the DMI term, which can be responsible for the coupling of (E_1^b, E_2^b) and (O_1^c, O_2^c). One of these interactions is the DM coupling between neighboring Mn^{3+} along the **c** axis:

$$\mathcal{H}_{\mathrm{DM}}^{E^b O^c} = \sum_i \alpha_{i,i+c/2}\left(S_i^b S_{i+c/2}^c - S_i^c S_{i+c/2}^b\right), \qquad (1)$$

where $\alpha_{i,i+c/2}$ changes sign under a translation by $\mathbf{c}/2$ and has a constant absolute value α. Such a term drives a uniform canting of the LTC *collinear* state with $E^a = 0$, $E^b \neq 0$, and $O^c = 0$ to a *noncollinear* state [39] with $E^a = 0$, $E^b \neq 0$, and $O^c \neq 0$ as shown in Fig. 9. We note that components of magnetic moments along **a** are allowed by symmetry. However, as they were not observed experimentally, they are not discussed here.

The microscopic interactions in Eq. (1) indicate that a collinear state with *E*-type sublattice magnetization purely along **b** (e.g., E_1^b) might be unstable toward a state described by a sublattice magnetization along the **c** of the O-type (e.g., O_1^c). Our measurements yield a $\pm 3.9^\circ$ angle between m^b and m^c, which is lower than the $\pm 9^\circ$ angle predicted using the coupling strength adopted by Mochizuki *et al.* [14]. The deviation of the tilting angles may arise because the MC simulations were performed with the strength of the couplings representative of $LaMnO_3$. Therefore, a definite deviation of the parameters in the case of $LuMnO_3$ with smaller *R* radii can be expected, inducing a variation in the tilting angle. Also, other magnetic interaction terms such as in-plane single-ion anisotropy comparable to the DMI terms cannot be neglected while predicting the tilting angle in the *bc* plane.

Monte Carlo simulations performed in Ref. [14] yielded a *noncollinear* magnetic structure where the *E*-type order along the **b** axis is strongly canted in the *ab* plane ($\phi \approx \pm 25^\circ$) and weakly canted in the *bc* plane ($\theta \approx \pm 9^\circ$). However, in our studies we only found evidence of the m_i^b and m_i^c components. This is evidence that the interactions responsible for stabilizing a tilting of moments in the *ab* plane are weak in *o*-$LuMnO_3$.

To investigate the interactions inducing the various types of canting and to obtain indications of their relative strength from the experimentally observed magnetic structure, we consider the same model Hamiltonian as discussed by Mochizuki *et al.* [14]. We restrict our analysis to the values of symmetric exchanges used therein, $J_b = 2.4$ meV [40]. We study the minimal energy state of such a model by numerically minimizing the Hamiltonian for a unit cell doubled along the **b** axis and with periodic boundary conditions in every crystallographic direction. The coupling of the spin to the phonon is traced out by minimizing analytically with respect to the lattice displacements. This yields a biquadratic coupling for the spin of the form $\mathcal{H}_{\mathrm{biq}} = \Gamma \sum_i (\mathbf{S}_i \cdot \mathbf{S}_{i+x})^2 + (\mathbf{S}_i \cdot \mathbf{S}_{i+y})^2$, where $\Gamma = -(J'_{ab})^2/(4\,\mathrm{K})$ as presented in Ref. [14].

The axes of single-ion anisotropy are determined by the position of the oxygens coordinating each of the four Mn^{3+} ions in the crystallographic unit cell. Here we consider the positions of the oxygen ions presented by Mochizuki *et al.* [14] noticing that the one obtained experimentally for our sample is relatively close to them. We tested the model with small deviations in the positions of the oxygen ions as obtained in $LuMnO_3$, but it failed to explain the discrepancy between the observed and calculated canting directions.

The strength of the single-ion anisotropy is determined by the two coupling constants [14] *E* and *D*. These coupling constants are defined in terms of spin components in the local tilted coordinate axes of the MnO_6 octahedron, as shown in Fig. 3 of Ref. [14]. *D* is associated with the anisotropy axis with a large **c** component and tiny *ab* plane components, which point mainly along **a**. Such an anisotropy for negative (positive) values of *D* favors the main component of the spins to be along (perpendicular to) the **c** direction. The coupling *E* is the

strength of the anisotropy axis, which has the main components in the ab plane. These axes are arranged in a staggered fashion.

Independently of its sign, E favors spins components both in the **a** and **c** directions. We note that to obtain a magnetic ground state with dominant component of spins along the **b** axis, the following scenarios have to be realized. For negative values of D, the term with strength E must be dominant, while for positive values of D, E can be small. Due to the orientation of the anisotropy axes associated with E, sizable values of the constants E (with respect to the size of the exchanges couplings) induce canting of spins toward the **a** axis. The canting of spins away from the *collinear* E-type magnetic moments along **b** is induced by the symmetry of the anisotropy axis in the unit cell and leads to a staggered magnetization along **a** and **c**.

The DM interactions between nearest-neighbor Mn^{3+} ions that are allowed by symmetry have their strength determined by five coupling constants, as was described in Ref. [38] and later used in Ref. [14]. The DM interactions between spins in the same ab plane are identified by the coupling constants $(\alpha_{ab},\beta_{ab},\gamma_{ab})$, and they are related to the Mn-O-Mn bonds as shown in Fig. 4 of Ref. [14]. The direction of the Dzyaloshinskii vectors associated with these constants changes in the unit cell. The way in which the Dzyaloshinskii vectors are staggered restricts the types of canting that the DM interaction can induce to the E-type magnetic order. In-plane DM interactions do not contribute to any canting when the magnetic unit cell is obtained by doubling chemical unit cells along the **b** direction. In particular, the contribution to the energy of the interaction associated with α_{ab} vanishes for states with wave vector $q_a = 0$. The interactions associated with β_{ab},γ_{ab} either do not favor spin canting away from the dominant component along **b**, or they favor states that are not compatible with $q_b = 0.5$, respectively. The DM interactions between Mn^{3+} neighbors along **c** favor sublattice magnetizations along **a** and **c** that have the same symmetry properties of E^b. When the interaction associated with α_c perturbs the E-type magnetic ordering along **b**, it induces a sublattice magnetization along **c** of the O^c type. The interactions associated with the coupling β_c do not couple to the magnetic moments along **b** and play a role only when canting from collinearity along **b** is induced by other couplings.

Figures 8(a) and 8(b) show, respectively, the E and α_c dependence of $|S^a|/|S^b|$ and $|S^c|/|S^b|$ in the numerically obtained ground state for the couplings used in Ref. [14]. The cantings obtained with the values of E and α_c used by Mochizuki *et al.* are marked by the black star, and they compare well with their result ($|S^a|/|S^b| \sim 0.5$ and $|S^c|/|S^b| \sim 0.17$). Figures 8(c) and 8(d) show the same ratio of spin components but for $\alpha_{ab} = \beta_{ab} = \gamma_{ab} = \beta_c = 0$. No clear variation in the landscape of $|S^a|/|S^b|$ and $|S^c|/|S^b|$ indicates the weak dependence of the cantings on the strength of such couplings. We note that the small discrepancy of the two cases at low values of E is related to extremely small cantings induced by β_c.

Furthermore, we note that the canting along the **a** direction is mainly controlled by the strength of E, while that along **c** is mainly controlled by the parameter α_c. This has two implications. First, there is an absence of experimental evidence for cantings along **a**, which means that the components of

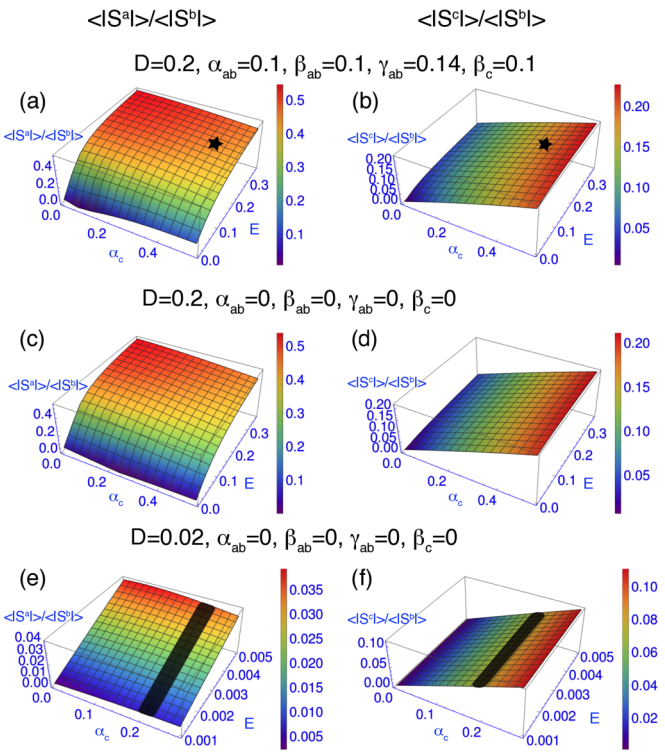

FIG. 8. E and α_c dependence of $|S^a|/|S^b|$ (left panels) and $|S^c|/|S^b|$ (right panels) in the ground-state spin configuration of the model described in Ref. [14], obtained as described in the text. Here, E and D represent the single-ion anisotropy in the ab plane and along the **c** axis, respectively, whereas (α,β,γ) are DM interactions in the ab plane and the **c** axis. The upper, middle, and lower panels show the results for different values of the relevant interactions with spin-orbit origin. The black star represents the canting size corresponding to the coupling parameters in Ref. [14]. The dark areas in (e),(f) represent the coupling strengths, which correspond to the experimentally observed canting of the magnetic moments. All the coupling strengths are presented in meV.

magnetic moments along **a** are smaller than the instrumental resolution ($(0.01\mu_B$ or, equivalently, 0.15 degrees). This implies that the value of E with respect to the exchange coupling constants is likely to be much smaller than that used by Mochizuki *et al.* [14]. Secondly, the observed canting of spins along the **c** direction implies that the value of α_c ($\approx$0.2 meV) is similar to that used in Ref. [14], albeit probably somewhat smaller. Such an imbalance in contributions from the single-ion anisotropy and the DM interactions is different from the results presented by Mochizuki *et al.* [14].

Figures 8(e) and 8(f) show the dependence of the $|S^a|/|S^b|$ and $|S^c|/|S^b|$ when the value of single-ion anisotropies is strongly reduced ($D = 0.02$ meV, $E \leqslant 0.005$ meV) while the α_c is kept to the same order of magnitude ($\leqslant$0.25 meV), which corresponds to the obtained ratio of the spin components in the bc plane. Clearly, when D is reduced, we do not observe any drastic change in the dependence of the canted components along **c**. Therefore, we propose that the incompatibility of the canting obtained by Mochizuki *et al.* [14] with those obtained experimentally relies on an overestimation of the role of single-ion anisotropy.

In contrast to the coexistence of E-type and cycloidal phase observed in o-$YMnO_3$ [13,18], for the low-temperature phase of o-$LuMnO_3$ we only observe reflections sensitive to a commensurate order. We note that, as mentioned above, there are DM interactions (i.e., those relative to the coupling γ_{ab}) that can favor states that are not compatible with $q_b = 0.5$. Therefore, we suggest that the presence of coexisting E-type and cycloidal antiferromagnetism might depend on the strength of a different coupling than the DM interaction (α_c) giving rise to the *noncollinearity* discussed here.

Recent studies of different $RMnO_3$ (R = Y, Ho, and Tm) with E-type magnetic ground state provide evidence of tilting of the Mn spins away from the *collinear* state similar to our results [41–43]. Furthermore, our results are consistent with recent studies of the magnetic phase of o-$LuMnO_3$ using resonant soft-x-ray scattering [44,45]. Our neutron diffraction measurements uniquely determine the symmetry of the magnetic order of the o-$LuMnO_3$, confirm the absence of a tilting toward the a axis in the commensurate phase, and thus provide information about the presence of antisymmetric interactions.

IV. CONCLUSION

Representation analysis was used to determine the magnetic structure in the incommensurate and commensurate magnetic phase of $LuMnO_3$. In the commensurate phase, the extent of the Mn moment tilting away from the **b** axis in the bc plane was determined, and direct evidence of the *noncollinear* E-type state was presented. An indication of the coupling between the magnetic and electric phase was confirmed from the concomitant presence of anomalies in the temperature dependence of the electric and the magnetic properties. Both microscopic and phenomenological analyses show that a DMI term can stabilize the spin canting in the ground-state E-type magnetic structure. Spin-lattice coupling giving rise to a large polarization, when compared to other multiferroic compounds, was demonstrated. $LuMnO_3$ can therefore be considered as an ideal candidate to study fundamental microscopic mechanisms essential for developing materials useful in technological devices.

ACKNOWLEDGMENTS

Work at the Paul Scherrer Institut (PSI) is supported by the Swiss National Science Foundation (Project No. 200021-147049). The work is based on experiments performed at the Swiss Spallation Neutron Source, SINQ, Paul Scherrer Institut, Switzerland. The authors wish to thank C. Joachim for helpful comments.

APPENDIX: SUBLATTICE MAGNETIZATIONS

The LTC phase is described by one of the two types of sublattice magnetization:

$$E_1 = E_2^a\,\hat{\mathbf{a}} + E_1^b\,\hat{\mathbf{b}} + \mathrm{O}_1^c\,\hat{\mathbf{c}},$$
$$E_2 = E_1^a\,\hat{\mathbf{a}} + E_2^b\,\hat{\mathbf{b}} + \mathrm{O}_2^c\,\hat{\mathbf{c}}, \quad \text{(A1)}$$

where E_i^b and O_i^c are the sum of the sublattice magnetization with the signs given in Table I, where $i = 1,2$ is the index used in the table. From the refinement, we cannot resolve any magnetic moment along the **a** direction. Henceforth, we neglect the first terms on the right-hand side of Eqs. (A1) ($E_i^a = 0$). We note that such a description of the basis vectors is possible as the pairs (E_2^a, E_1^a) [46], (E_1^b, E_2^b), and $(\mathrm{O}_1^c, \mathrm{O}_2^c)$ transform in the same way under the generators of the *Pbnm* paramagnetic space group (see Table II).

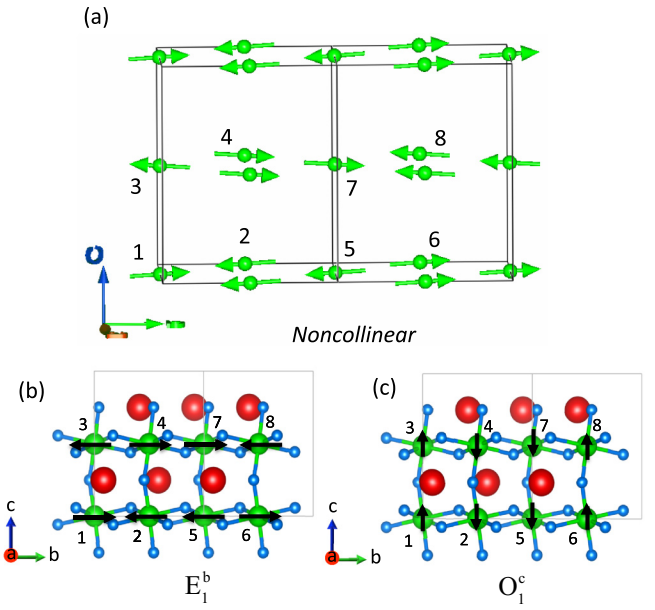

FIG. 9. (a) The refined magnetic structure of $LuMnO_3$ in the commensurate phase (FPstudio) [22]. Here, we show the spin structure of the *noncollinear* E_1 domain. (b) Schematic illustration of the spin structure projected on the bc plane defined by sublattice magnetization along the **b** axis (E_1^b) and (c) along the **c** axis (O_1^c). Lu (red), Mn (green), and O (blue) ions are represented by solid spheres. Black arrows here resemble magnetization components.

Therefore, the magnetic structure can be described by what follows. The **b** components of magnetic moments of adjacent Mn^{3+} ions along the **b** direction in a given ab plane (say $c = 0$) are arranged as ↑↑↓↓. On the neighboring Mn^{3+} of the next ab layer (say $c = 1/2$), the **b** components of the magnetic moments are reversed (i.e., ↓↓↑↑). The arrangements of the **c** components of the magnetic moments are different. Within the same ab plane (say $c = 0$) they also have an ↑↑↓↓ staggered magnetization. However, this repeats identically in the next ab layers along the **c** direction (say $c = 1/2$). Thus, the *noncollinear* E-type (Fig. 9) differs from the *collinear* E-type [Fig. 9(b)] in relation to sublattice magnetization along the **b** and **c** axes.

TABLE II. Transformation of the sublattice magnetization along **b** and along **c** (see Table I) under the generators of the space group $Pbnm$. Here 2_a and 2_c refer, respectively, to the twofold rotations along **a** and **c** followed by the appropriate translations. I and T indicate space inversion and time reversal, respectively.

	2_a	2_c	I	T
$\begin{pmatrix} E_1^b \\ E_2^b \end{pmatrix}$	$\begin{pmatrix} -1 & 0 \\ 0 & 1 \end{pmatrix}$	$\begin{pmatrix} 0 & 1 \\ 1 & 0 \end{pmatrix}$	$\begin{pmatrix} 0 & 1 \\ 1 & 0 \end{pmatrix}$	$\begin{pmatrix} -1 & 0 \\ 0 & -1 \end{pmatrix}$
$\begin{pmatrix} O_1^c \\ O_2^c \end{pmatrix}$	$\begin{pmatrix} -1 & 0 \\ 0 & 1 \end{pmatrix}$	$\begin{pmatrix} 0 & 1 \\ 1 & 0 \end{pmatrix}$	$\begin{pmatrix} 0 & 1 \\ 1 & 0 \end{pmatrix}$	$\begin{pmatrix} -1 & 0 \\ 0 & -1 \end{pmatrix}$

[1] N. A. Spaldin and M. Fiebig, Science **309**, 391 (2005).

[2] G. Catalan and J. F. Scott, Adv. Mater. **21**, 2463 (2009).

[3] L. W. Martin, S. P. Crane, Y.-H. Chu, M. B. Holcomb, M. Gajek, M. Huijben, C.-H. Yang, N. Balke, and R. Ramesh, J. Phys.: Condens. Matter **20**, 434220 (2008).

[4] T. Kimura, T. Goto, H. Shintani, K. Ishizaka, T. Arima, and Y. Tokura, Nature (London) **426**, 55 (2003).

[5] M. Kenzelmann, A. B. Harris, S. Jonas, C. Broholm, J. Schefer, S. B. Kim, C. L. Zhang, S.-W. Cheong, O. P. Vajk, and J. W. Lynn, Phys. Rev. Lett. **95**, 087206 (2005).

[6] T. Kimura, G. Lawes, T. Goto, Y. Tokura, and A. P. Ramirez, Phys. Rev. B **71**, 224425 (2005).

[7] D. Senff, P. Link, N. Aliouane, D. N. Argyriou, and M. Braden, Phys. Rev. B **77**, 174419 (2008).

[8] M. Matsubara, S. Manz, M. Mochizuki, T. Kubacka, A. Iyama, N. Aliouane, T. Kimura, S. L. Johnson, D. Meier, and M. Fiebig, Science **348**, 1112 (2015).

[9] V. Y. Pomjakushin, M. Kenzelmann, A. Dönni, A. B. Harris, T. Nakajima, S. Mitsuda, M. Tachibana, L. Keller, J. Mesot, H. Kitazawa, and E. Takayama-Muromachi, New J. Phys. **11**, 043019 (2009).

[10] A. Muñoz, M. T. Casàis, J. A. Alonso, M. J. Martí-nez-Lope, J. L. Martí-nez, and M. T. Fernández-Díaz, Inorg. Chem. **40**, 1020 (2001).

[11] A. Muñoz, J. A. Alonso, M. T. Casais, M. J. Martí-nez-Lope, J. L. Martí-nez, and M. T. Fernández-Díaz, J. Phys.: Condens. Matter **14**, 3285 (2002).

[12] S. Ishiwata, Y. Tokunaga, Y. Taguchi, and Y. Tokura, J. Am. Chem. Soc. **133**, 13818 (2011).

[13] D. Okuyama, S. Ishiwata, Y. Takahashi, K. Yamauchi, S. Picozzi, K. Sugimoto, H. Sakai, M. Takata, R. Shimano, Y. Taguchi, T. Arima, and Y. Tokura, Phys. Rev. B **84**, 054440 (2011).

[14] M. Mochizuki, N. Furukawa, and N. Nagaosa, Phys. Rev. B **84**, 144409 (2011).

[15] T. Aoyama, K. Yamauchi, A. Iyama, S. Picozzi, K. Shimizu, and T. Kimura, Nat. Commun. **5**, 4927 (2014).

[16] N. Terada, D. D. Khalyavin, P. Manuel, T. Osakabe, A. Kikkawa, and H. Kitazawa, Phys. Rev. B **93**, 081104 (2016).

[17] H. Okamoto, N. Imamura, B. Hauback, M. Karppinen, H. Yamauchi, and H. Fjellvåg, Solid State Commun. **146**, 152 (2008).

[18] S. Ishiwata, Y. Kaneko, Y. Tokunaga, Y. Taguchi, T.-h. Arima, and Y. Tokura, Phys. Rev. B **81**, 100411 (2010).

[19] Y. S. Chai, Y. S. Oh, L. J. Wang, N. Manivannan, S. M. Feng, Y. S. Yang, L. Q. Yan, C. Q. Jin, and K. H. Kim, Phys. Rev. B **85**, 184406 (2012).

[20] M. Tachibana, T. Shimoyama, H. Kawaji, T. Atake, and E. Takayama-Muromachi, Phys. Rev. B **75**, 144425 (2007).

[21] P. Fischer, G. Frey, M. Koch, M. Könnecke, V. Pomjakushin, J. Schefer, R. Thut, N. Schlumpf, R. Bürge, U. Greuter, S. Bondt, and E. Berruyer, Physica B **276-278**, 146 (2000).

[22] J. Rodriguez-Carvajal, Physica B **192**, 55 (1993); www.ill.eu/sites/fullprof/.

[23] H. T. Stokes and D. M. Hatch, *Isotropy Subgroups of the 230 Crystallographic Space Groups* (World Scientific, Singapore, 1988); Isotropy software suite, iso.byu.edu.

[24] B. J. Campbell, H. T. Stokes, D. E. Tanner, and D. M. Hatch, J. Appl. Crystallogr. **39**, 607 (2006).

[25] T. Goto, T. Kimura, G. Lawes, A. P. Ramirez, and Y. Tokura, Phys. Rev. Lett. **92**, 257201 (2004).

[26] Y. Hu, C. N. Borca, E. Kleymenov, M. Nachtegaal, B. Delley, M. Janousch, A. Dönni, M. Tachibana, H. Kitazawa, E. Takayama-Muromachi, M. Kenzelmann, C. Niedermayer, T. Lippert, A. Wokaun, and C. W. Schneider, Appl. Phys. Lett. **100**, 252901 (2012).

[27] T. Kimura, S. Ishihara, H. Shintani, T. Arima, K. T. Takahashi, K. Ishizaka, and Y. Tokura, Phys. Rev. B **68**, 060403 (2003).

[28] O. Kovalev, in *Representations of the Crystallographic Space Groups*, edited by H. T. Stokes and D. M. Hatch (Gordon and Breach, London, 1993).

[29] R. Ramesh and N. A. Spaldin, Nat. Mater. **6**, 21 (2007).

[30] S. M. Disseler, J. A. Borchers, C. M. Brooks, J. A. Mundy, J. A. Moyer, D. A. Hillsberry, E. L. Thies, D. A. Tenne, J. Heron, M. E. Holtz, J. D. Clarkson, G. M. Stiehl, P. Schiffer, D. A. Muller, D. G. Schlom, and W. D. Ratcliff, Phys. Rev. Lett. **114**, 217602 (2015).

[31] J. R. Sahu, C. R. Serrao, N. Ray, U. V. Waghmare, and C. N. R. Rao, J. Mater. Chem. **17**, 42 (2007).

[32] O. L. Makarova, I. Mirebeau, S. E. Kichanov, J. Rodriguez-Carvajal, and A. Forget, Phys. Rev. B **84**, 020408 (2011).

[33] M. D. Kuzmin, L. M. García, M. Artigas, and J. Bartolomé, Phys. Rev. B **54**, 4093 (1996).

[34] S. Picozzi, K. Yamauchi, B. Sanyal, I. A. Sergienko, and E. Dagotto, Phys. Rev. Lett. **99**, 227201 (2007).

[35] M. Mostovoy, Phys. Rev. Lett. **96**, 067601 (2006).

[36] I. A. Sergienko, C. Şen, and E. Dagotto, Phys. Rev. Lett. **97**, 227204 (2006).

[37] M. Mochizuki and N. Furukawa, Phys. Rev. B **80**, 134416 (2009).

[38] I. Solovyev, N. Hamada, and K. Terakura, Phys. Rev. Lett. **76**, 4825 (1996).

[39] We cannot exclude the contributions from other microscopic interactions such as single-ion anisotropy terms, which can stabilize the *noncollinear E*-type order.

[40] Throughout the paper, we use the same nomenclature of the coupling constants used in Ref. [14].

[41] Y. W. Windsor, M. Ramakrishnan, L. Rettig, A. Alberca, E. M. Bothschafter, U. Staub, K. Shimamoto, Y. Hu, T. Lippert, and C. W. Schneider, Phys. Rev. B **91**, 235144 (2015).

[42] K. Shimamoto, Y. W. Windsor, Y. Hu, M. Ramakrishnan, A. Alberca, E. M. Bothschafter, L. Rettig, T. Lippert, U. Staub, and C. W. Schneider, Appl. Phys. Lett. **108**, 112904 (2016).

[43] H. Wadati, J. Okamoto, M. Garganourakis, V. Scagnoli, U. Staub, Y. Yamasaki, H. Nakao, Y. Murakami, M. Mochizuki, M. Nakamura, M. Kawasaki, and Y. Tokura, Phys. Rev. Lett. **108**, 047203 (2012).

[44] M. Garganourakis, Y. Bodenthin, R. A. de Souza, V. Scagnoli, A. Dönni, M. Tachibana, H. Kitazawa, E. Takayama-Muromachi, and U. Staub, Phys. Rev. B **86**, 054425 (2012).

[45] Y. W. Windsor, S. W. Huang, Y. Hu, L. Rettig, A. Alberca, K. Shimamoto, V. Scagnoli, T. Lippert, C. W. Schneider, and U. Staub, Phys. Rev. Lett. **113**, 167202 (2014).

[46] (E_2^a, E_1^a) transforms in the same way as (E_1^b, E_2^b), and the expected ordering of sublattice magnetization along the a axis would be expressed in the same way as along the b axis but with the subscript that represents the domains being swapped.